Am J Physiol Cell Physiol 314: C721–C731, 2018.
First published March 7, 2018; doi:10.1152/ajpcell.00184.2017.

RESEARCH ARTICLE | *Cell-to-Cell Communication and Signaling Pathways*

Reactive oxygen species upregulate expression of muscle atrophy-associated ubiquitin ligase Cbl-b in rat L6 skeletal muscle cells

Takayuki Uchida,[1] Yoshihiro Sakashita,[1] Kanako Kitahata,[1] Yui Yamashita,[1] Chisato Tomida,[1] Yuki Kimori,[1] Akio Komatsu,[1] Katsuya Hirasaka,[1,2] Ayako Ohno,[1] Reiko Nakao,[1,3] Atsushi Higashitani,[4] Akira Higashibata,[5] Noriaki Ishioka,[5] Toru Shimazu,[6] Takeshi Kobayashi,[7] Yuushi Okumura,[1,8] Inho Choi,[9] Motoko Oarada,[8] Edward M. Mills,[10] Shigetada Teshima-Kondo,[1,11] Shin'ichi Takeda,[12] Eiji Tanaka,[13] Keiji Tanaka,[14] Masahiro Sokabe,[7] and Takeshi Nikawa[1]

[1]*Department of Nutritional Physiology, Institute of Medical Nutrition, Tokushima University Graduate School, Tokushima, Japan;* [2]*Graduate School of Fisheries Science and Environmental Studies, Nagasaki University, Nagasaki, Japan;* [3]*Biological Clock Research Group, Biomedical Research Institute, National Institute of Advanced Industrial Science and Technology, Tsukuba, Ibaraki, Japan;* [4]*Graduate School of Life Sciences, Tohoku University, Sendai, Japan;* [5]*Institute of Space and Astronautical Science, Japan Aerospace Exploration Agency, Tsukuba, Ibaraki, Japan;* [6]*Japan Space Forum, Tokyo, Japan;* [7]*Department of Physiology, Nagoya University, School of Medicine, Nagoya, Japan;* [8]*Faculty of Nutritional Science, Sagami Women's University, Kanagawa, Japan;* [9]*Institute of Space Biology, Yonsei University, Wonju, South Korea;* [10]*Division of Pharmacology/Toxicology, College of Pharmacy, University of Texas, Austin, Texas;* [11]*Department of Nutrition, Graduate School of Comprehensive Rehabilitation, Osaka Prefecture University, Osaka, Japan;* [12]*Translational Research Center, National Center of Neurology and Psychiatry, Tokyo, Japan;* [13]*Department of Orthodontic Dentistry, Institute of Medical Biosciences, Tokushima University Graduate School, Tokushima, Japan; and* [14]*Tokyo Metropolitan Institute of Medical Science, Tokyo, Japan*

Submitted 14 August 2017; accepted in final form 26 February 2018

Uchida T, Sakashita Y, Kitahata K, Yamashita Y, Tomida C, Kimori Y, Komatsu A, Hirasaka K, Ohno A, Nakao R, Higashitani A, Higashibata A, Ishioka N, Shimazu T, Kobayashi T, Okumura Y, Choi I, Oarada M, Mills EM, Teshima-Kondo S, Takeda S, Tanaka E, Tanaka K, Sokabe M, Nikawa T. Reactive oxygen species upregulate expression of muscle atrophy-associated ubiquitin ligase Cbl-b in rat L6 skeletal muscle cells. *Am J Physiol Cell Physiol* 314: C721–C731, 2018. First published March 7, 2018; doi:10.1152/ajpcell.00184.2017.—Unloading-mediated muscle atrophy is associated with increased reactive oxygen species (ROS) production. We previously demonstrated that elevated ubiquitin ligase casitas B-lineage lymphoma-b (Cbl-b) resulted in the loss of muscle volume (Nakao R, Hirasaka K, Goto J, Ishidoh K, Yamada C, Ohno A, Okumura Y, Nonaka I, Yasutomo K, Baldwin KM, Kominami E, Higashibata A, Nagano K, Tanaka K, Yasui N, Mills EM, Takeda S, Nikawa T. *Mol Cell Biol* 29: 4798–4811, 2009). However, the pathological role of ROS production associated with unloading-mediated muscle atrophy still remains unknown. Here, we showed that the ROS-mediated signal transduction caused by microgravity or its simulation contributes to Cbl-b expression. In L6 myotubes, the assessment of redox status revealed that oxidized glutathione was increased under microgravity conditions, and simulated microgravity caused a burst of ROS, implicating ROS as a critical upstream mediator linking to downstream atrophic signaling. ROS generation activated the ERK1/2 early-growth response protein (Egr)1/2-Cbl-b signaling pathway, an established contributing pathway to muscle volume loss. Interestingly, antioxidant treatments such as *N*-acetylcysteine and TEMPOL, but not catalase, blocked the clinorotation-mediated activation of ERK1/2. The increased ROS induced transcriptional activity of Egr1 and/or Egr2 to stimulate Cbl-b expression through the ERK1/2 pathway in L6 myoblasts, since treatment with Egr1/2 siRNA and an ERK1/2 inhibitor significantly suppressed clinorotation-induced Cbl-b and Egr expression, respectively. Promoter and gel mobility shift assays revealed that Cbl-b was upregulated via an Egr consensus oxidative responsive element at −110 to −60 bp of the Cbl-b promoter. Together, this indicates that under microgravity conditions, elevated ROS may be a crucial mechanotransducer in skeletal muscle cells, regulating muscle mass through Cbl-b expression activated by the ERK-Egr signaling pathway.

Egr; rat L6 cells; ROS; ubiquitin ligase Cbl-b; unloading-mediated muscle atrophy

INTRODUCTION

Mechanotransduction is the transformation of physical stress into biochemical signals (32). Skeletal muscle atrophy is a response to decreased physical signals (unloading), such as under microgravity, bed rest, and neural inactivation, and is characterized by muscle volume loss and muscle fiber-type switching (1, 31). We previously reported that spaceflight, denervation, and tail suspension upregulated the expression of various muscle atrophy-related genes in rat gastrocnemius muscle compared with the respective control conditions (20). However, the pathways regulating the initial changes in the biochemical properties of skeletal muscle cells under mechanical unloading conditions and how the responses of these cells are achieved remain unclear.

Understanding the molecular basis of mechanotransduction is impossible without knowing the impact of mechanical unloading on skeletal muscle. Our recent research has focused on

Address for reprint requests and other correspondence: T. Nikawa, Department of Nutritional Physiology, Institute of Medical Nutrition, Tokushima University Graduate School 3-18-15, Kuramoto-cho, Tokushima 770-8503, Japan (e-mail: nikawa@tokushima-u.ac.jp).

this issue. In muscle volume loss, insulin-like growth factor 1 (IGF-I) signaling was crucial for both proteolysis and synthesis (20, 29, 31). We also demonstrated that the ubiquitin-proteasome system was important in the unloading environment (12, 19). In particular, ubiquitin ligase casitas B-lineage lymphoma-b (Cbl-b), which is highly expressed under unloading conditions, caused ubiquitination and subsequent degradation of insulin receptor substrate 1 (IRS-1). This Cbl-b-mediated degradation of IRS-1 contributed to dysregulated IGF-I signaling under unloading conditions, leading to skeletal muscle atrophy (12, 19, 29). However, the factors that stimulate Cbl-b expression in skeletal muscle cells exposed to unloading stress have remained unknown.

Previous studies have established that unloading-mediated muscle atrophy is associated with mitochondrial dysfunction and increased reactive oxygen species (ROS) production (24). Indeed, administration of cysteine, an antioxidative nutrient, suppressed the degradation of myosin heavy chain (MyHC) in association with redox regulation in gastrocnemius muscle of tail-suspended rats (11). Prevention of increased ROS production in human diaphragm during mechanical ventilation and bed rest also protected diaphragmatic mitochondria from damage and respiratory dysfunction (23). Furthermore, attenuation of nitric oxide imbalance suppressed the *S*-nitrosylation of calcium release/uptake proteins such as ryanodine receptor 1 and sarco/endoplasmic reticulum Ca^{2+}-ATPase in mitochondrial-associated membranes (28).

In the present study, we subjected rat L6 myotubes to cultivation at the International Space Station (ISS) for 10 days to clarify the initial response to microgravity conditions. We first found evidence for cumulative oxidative stress in myotubes cultured under microgravity conditions. This finding led us to hypothesize the importance of ROS as mechanotransducers for unloading-mediated muscle atrophy. In addition, we identified a signaling pathway in which ROS induced the early growth response protein (Egr) axis leading to Cbl-b expression.

MATERIALS AND METHODS

Cell culture. Rat myoblastic L6 skeletal muscle cells (CRL-1458; ATCC) and COS7 cells (CRL-1651; ATCC) were maintained in DMEM containing 10% FBS and 1% penicillin-streptomycin mixed solution (Nacalai Tesque, Kyoto, Japan) at 37°C in 5% CO_2/95% air. The ERK1/2 inhibitor PD-98059 was purchased from Cell Signaling Technology (Danvers, MA). *N*-acetylcysteine (NAC), 1-oxyl-2,2,6,6-tetramethyl-4-hydroxypiperidine (TEMPOL), and catalase were all purchased from Sigma (St. Louis, MO).

Space experiment (Myo-Lab project). An overview and schematic of the space experiment is shown in Fig. 1. L6 cells at 100% confluence were fused by shifting the medium to a differentiation medium, i.e., DMEM containing 0.5% FBS. Three days later, we confirmed the differentiation stage by immunoblotting for MyHC and myogenin (data not shown) (9). After differentiation for 5 day, the cells were launched at the Kennedy Space Center in the ISS on April 5, 2010 (STS-131). On the 7th day after launch, culture medium was replaced with fresh DMEM with or without 40 ng/ml IGF-1 (Sigma), and cells were cultured for 10 days under microgravity or 1*G* conditions, the latter achieved by centrifugation. In orbit, cells were preserved after harvest with RNA Later (Qiagen, Venlo, The Netherlands) and stored at −80°C in the deep freezer of the Japanese Experimental Module (JEM). Once returned to earth, samples were kept at −80°C until analysis.

Three-dimensional clinorotation. As an in vitro model of unloading conditions, we subjected cultures of rat L6 cells to a three-dimensional

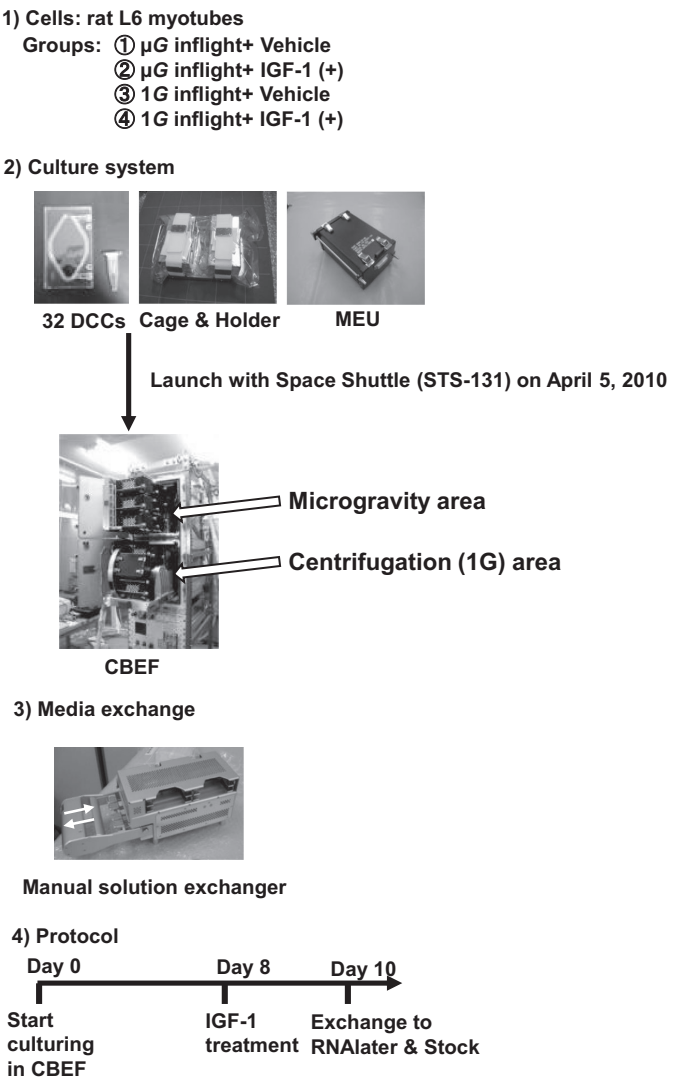

Fig. 1. Myo-Lab cell biology space experiment. *1*) Culture system. Rat L6 myoblasts (1×10^5 cells) were seeded on disposable culturing chambers (DCCs) 7 days before launch and differentiated into myotubes with DMEM supplemented with 0.5% FBS. DCCs were enclosed with an Anaero Pack, a chemical CO_2 producer in a polyethylene back, cage, and hanger. The DCCs were covered with a measurement experiment unit (MEU) and launched with Space Shuttle Discovery (STS-131) on April 5, 2010. *2*) After docking with the International Space Station (ISS), L6 cells were divided into microgravity and 1*G* control groups. Cells in each group were cultured with or without IGF-I treatment in the microgravity or centrifugation areas of the Cell Biology Experiment Facility (CBEF), a CO_2 incubator in the ISS. *3*) Finally, medium was replaced with RNAlater using a manual solution exchanger and cooled to −80°C for storage. *4*) Timeline for the protocol at ISS.

(3D) clinorotator (Advanced Engineering Services, Tokyo, Japan), as described previously (9). Disposable cell cassettes (DCCs) containing L6 cells at ~30 or 75% confluence were filled with DMEM containing 10% FBS (proliferation medium) or 0.5% FBS (differentiation medium), respectively. The cassettes were rotated around two axes on the 3D clinorotator at 37°C in a 5% CO_2 chamber. The rate and cycle of rotation were controlled by the computer to randomize the gravity vector in both magnitude and direction, and then the dynamic stimulation of gravity to cells was cancelled in any direction, simulating microgravity conditions. Reagents and media in the DCCs were not changed during rotation. Control cells were incubated in parallel under the same conditions but were not subjected to rotation.

Table 1. *Primer sequences used for PCR*

Gene	Sequence	Length, bp
Cbl-b (human), −2,072 to +249 bp		
Sense	5′-CACCACCCTGGTTGTCCACAGG-3′	
Antisense	5′-CTTTCGGCGCCGTAGCTGTCCA-3′	
Cbl-b (human), −111 to +249 bp		
Sense	5′-CACCGAGCTCGGCATTGGCTCA-3′	
Antisense	5′-CTTTCGGCGCCGTAGCTGTCCA-3′	
Cbl-b (human), −59 to +249 bp		
Sense	5′-CACCGGTACCCTGGGTCCTGT-3′	
Antisense	5′-CTTTCGGCGCCGTAGCTGTCCA-3′	
Cbl-b (rat)		
Sense	5′-GAAGGGTGAAGATGCTTTTGATG-3′	333
Antisense	5′-TGATGAATTTCTGGTGCAGTCCT-3′	
Egr1 (rat)		
Sense	5′-GAGGAGATGATGCTGCTGAG-3′	95
Antisense	5′-CTGCTGCTGCTGCTGTTATT-3′	
Egr2 (rat)		
Sense	5′-CCTCCAGCTTCAACCACAG-3′	100
Antisense	5′-GCTGAGTCTGGGACATGGTA-3′	
Egr3 (rat)		
Sense	5′-CTCAGTACGCAGACGACCAC-3′	99
Antisense	5′-GTCGCCGCAGTTGGAATAG-3′	
GAPDH (rat)		
Sense	5′-CGTGTTCCTACCCCCAATGT-3′	74
Antisense	5′-ATGTCATCATACTTGGCAGGTTTCT-3′	

Cbl-b, casitas B-lineage lymphoma-b; Egr1, -2, and -3, early-growth response proteins 1, 2, and 3, respectively.

Measurement of L6 myotube diameters. We took 10 photos per DCC at the high-power field on a BIOREVO, BZ-9000 (Keyence, Osaka, Japan). We selected myotubes with a length of >100 μm and measured the diameter at the middle portion of the myotube with a software BZ-II analyzer, as described previously (9). We measured the diameters of 100 myotubes/group.

Immunoblotting. Proteins (10 μg/lane) obtained from cell homogenates were subjected to immunoblotting. Protein concentration was determined by Lowry's method with bovine serum albumin as a standard (16), and immunoblot analyses were performed as described previously (9). The following antibodies were used: anti-Sp1 (sc-59; Santa Cruz Biotechnology, Dallas, TX), anti-α-tubulin (T5186), anti-myosin slow (M8421), anti-myosin fast (M1570), anti-mouse IgG (M9044; Sigma), anti-Egr 1 (ab208780), anti-Egr 2 (ab108399; Abcam, Cambridge, UK), anti-Cbl-b (no. 9498), anti-α-actinin (no. 6487), anti-phosphorylated ERK1/2, ERK (no. 4370), anti-ERK (no. 4695), anti-phosphorylated JNK (no. 4668), anti-JNK (no. 9252), anti-phosphorylated p38 (no. 4511), anti-p38 (#8690), and anti-rabbit IgG (no. 7074) (Cell Signaling Technology) antibodies.

Measurement of reduced and oxidized glutathione. To measure the level of GSH and GSSG in L6 cells, the cell extracts were subjected to A-7100 capillary electrophoresis and A-6100 mass spectrometry (CE-MS) system (Agilent Technologies, Tokyo, Japan).

ROS detection. ROS were detected with 2.5 μM of the oxidative stress-quenching immunofluorescence reagent CellROX Deep Red (Thermo Fisher Scientific, Waltham, MA) according to the manufacturer's instructions. L6 cells were pretreated with the reagent in media for 30 min before 3D clinorotation or treatment with 50 μM hydrogen peroxide (H_2O_2). After treatment, cells were washed by HBSS twice and then observed by a fluorescence microscope, i.e., BIOREVO, BZ-9000 (Keyence). The images were quantified by an image analysis software (ImageJ; National Institutes of Health, Bethesda, MD).

Flow cytometry for ROS detection. L6 cells were grown to ~70% confluency in 12-well plates and subjected to clinorotation for 24 h. For comparison groups, cells were treated with vehicle [dimethyl sulfoxide (DMSO)], 10 μM H_2O_2, or 50 μM 1,1-diethyl-2-hydroxy-2-nitrosohydrazine (diethylamine NONOate) (Sigma) for 1 h at 37°C. Cells were harvested, resuspended, and incubated in HBSS with 5 μM 2′,7′-dichlorodihydrofluorescein diacetate (H2DCFDA) (Thermo Fisher Scientific) or 5 μM diaminofluorescein-2 diacetate (DAF-2 DA; Goryo Chemical, Sapporo, Japan). After incubation, cells were stained with 1 μg/ml propidium iodide (Dojindo, Kumamoto, Japan), and fluorescence was measured by a flow cytometer (Beckman Coulter, Brea, CA).

Luciferase assay. The human Cbl-b promoter sequences in the 5′-upstream untranslated region of exon 1 were amplified from chromosomal DNA with the synthetic primers shown in Table 1. The PCR products were digested with appropriate restriction enzymes and subcloned upstream of the firefly luciferase gene in the pGL3-Basic Vector (Promega, Fitchburg, WI). PCR products were confirmed based on their size, as determined by electrophoresis, and DNA sequencing. COS7 cells cultured in serum-free DMEM were transfected with plasmids containing the Cbl-b promoter luciferase constructs and then treated with vehicle (PBS) or 10 μM H_2O_2 for 24 h. Luciferase activity was measured using the manufacturer's protocol (Promega) and expressed as an average of the values from three independent experiments.

EMSA. Nuclear extracts were prepared from COS7 cells treated with or without H_2O_2. Binding reaction mixtures of nuclear extracts with synthetic DNA probes were incubated for 30 min at 22°C, as described previously (9). In supershift studies, 1 μl of the indicated affinity-purified rabbit anti-peptide antibodies (Santa Cruz Biotechnology, Santa Cruz, CA) was incubated with the extracts for 15 min before addition of the probe. Samples were resolved by electrophoresis on a 6% nondenaturing polyacrylamide gel, and gels were vacuum dried at 80°C for 1 h before visualization by autoradiography.

Quantitative RT-PCR. Real-time RT-PCR was performed with the Power SYBR Green PCR Master Mix (Thermo Fischer Scientific) using an Applied Biosystems 7300 Real-Time PCR System (Thermo Fischer Scientific), as described previously (21). The oligonucleotide primers used for amplification are listed in Table 1.

Small interfering RNAs and transfection. The 21-nucleotide small-interfering RNA (siRNA) triplexes for Egr 1 and Egr 2 were purchased from B-Bridge International (Tokyo, Japan), and the sequences are shown in Table 2. Negative control siRNA was purchased from Ambion (Austin, TX). L6 cells (40–60% confluence) were transfected using the jetPRIME kit (Polyplus, Berkeley, CA), as described previously (9).

Statistical analysis. All data were statistically evaluated by ANOVA using Statistical Package for Social Sciences software (release 6.1; SPSS Japan). Data are expressed as means ± SD. Differ-

Table 2. *siRNA sequences*

Target Gene	Sequence
siRNA for Egr1 (rat)	
Sense	5′-CAGCCUAGUCAGUGGCCUUTT-3′
Antisense	5′-AAGGCCACUGACUAGGCUGTT-3′
Sense	5′-CGCAAGAGGCAUACCAAAATT-3′
Antisense	5′-UUUUGGUAUGCCUCUUGCGTT-3′
Sense	5′-AGGGAAUGAAAGAGAGCAATT-3′
Antisense	5′-UUGCUCUCUUUCAUUCCCUTT-3′
siRNA for Egr2 (rat)	
Sense	5′-CGCCAAGGCCGUAGACAAATT-3′
Antisense	5′-UUUGUCUACGGCCUUGGCGTT-3′
Sense	5′-CCAGAAGGCAUCAUCAAUATT-3′
Antisense	5′-UAUUGAUGAUGCCUUCUGGTT-3′
Sense	5′-GAGCAAGGACAGCGAAAAATT-3′
Antisense	5′-UUUUUCGCUGUCCUUGCUCTT-3′

siRNA, small-interfering RNA.

ences between or among groups were analyzed with Scheffé's test. Differences were considered significant at $P < 0.05$.

RESULTS

Cumulative oxidative stress in L6 myocytes cultured under microgravity or simulated microgravity conditions. We cultured L6 myotubes (with >80% of the estimated fusion ratio of the myoblast/myotube) for 10 days in the JEM of the ISS and found that microgravity significantly decreased the thickness of L6 myotubes compared with myotubes under 1*G* inflight conditions (Fig. 2*A*). We also confirmed that 3D clinorotation significantly decreased myotube thickness compared with sedentary myotubes (Fig. 2*B*), which was similar to the effects of culturing on the ISS. To determine whether microgravity stimulated the degradation of myofiber proteins, we measured the levels of slow-type and fast-type MyHC proteins in myotubes cultured in microgravity or 1*G* inflight conditions (Fig. 2*C*). As expected, microgravity decreased levels of both MyHC proteins in L6 myotubes. There is a possibility that microgravity and clinorotation cause shear stress on cells during cultivation. We therefore also measured the level of α-actinin, since shear stress affects the amounts of cross-linking cytoskeletal proteins such as α-actinin in various cells (13). Microgravity and clinorotation had little impact on the amounts of α-actinin (Fig. 2*C*), indicating that real and simulated microgravity conditions in this study did not cause shear stress.

Under 1*G* conditions, only low levels of the reduced form of GSH were detected in L6 myotubes, and these levels were significantly increased by IGF-I treatment (Fig. 2*D*). Under microgravity conditions, GSH was not detectable in L6 cells even after IGF-I treatment. In contrast, GSSG, the oxidized form of GSH, was not detectable in L6 cells under 1*G* conditions, whereas it was detected under microgravity conditions only with IGF-I treatment. These findings suggest that microgravity conditions cause oxidative stress in L6 cells.

To confirm the oxidative stress induced by microgravity, we measured ROS production in L6 myotubes subjected to 3D clinorotation. Staining with CellROX Deep Red, a general oxidative stress indicator, revealed that 3D clinorotation induced significant oxidative stress in the cells to a similar extent as L6 myotubes treated with H_2O_2 (Fig. 2*E*). Flow cytometry with H2DCFDA, another general oxidative stress indicator, and DAF-2 DA, a nitric oxide-specific indicator, also showed that clinorotation as well as H_2O_2 treatment induced oxidative stress in L6 cells but that this oxidative stress was not due to the accumulation of NO (Fig. 2*F*). These findings are consistent with our previous report showing that cysteine supplementation prevented unloading-mediated decrease in rat hindlimb skeletal muscle wet weights (11).

Oxidative stress-mediated Cbl-b expression. We previously reported that exogenous ROS significantly upregulated Cbl-b expression in rat skeletal muscle (20). Therefore, we next investigated the mechanism of ROS-mediated regulation of Cbl-b expression by promoter mapping using truncated versions of the 5′ upstream untranslated region of exon 1 linked to the luciferase gene. As shown in Fig. 3*A*, H_2O_2 activated luciferase expression in reporters driven by promoter fragments −2,072 to +249 bp, −292 to +249 bp, and −111 to +249 bp but not by the construct containing the region −59 to +249 bp, indicating that the ROS-sensitive region was between −111 and −60 bp.

To identify the DNA-binding factors regulating this promoter, we used three probe sequences targeting the −111 to −92 (probe 1), −93 to −74 (probe 2), and −79 to −60 regions (probe 3) of the Cbl-b promoter region (Fig. 3B). These three regions contain consensus motifs for the cAMP-responsive element-binding factor (CRF), metal-responsive element-binding protein (MRE-BP), and the Egr 1 and Egr 2 transcription factors. Using EMSA, we observed no H_2O_2-inducible DNA-binding complexes with probes 1 and 2 in COS7 cells, suggesting that CRF and MRE-BP do not mediate the oxidative stress response of the Cbl-b promoter (Fig. 3, A and B). In contrast, we found that probe 3 mobility was highly sensitive to ROS. Furthermore, mutation of the second Egr 1/2 binding site in probe 3 (probe 3-mt2), but not the first Egr1/2 binding site (probe 3-mt1), decreased the formation of H_2O_2-inducible DNA-binding complexes. In addition, supershift assays using anti-Egr (Egr1 or/and -2) or anti-Sp1 antibodies showed that the density of bands was reduced by treatment with anti-Egr1 or -2 antibody but was unaffected by anti-Sp1 antibody, suggesting that Egr1 and -2 proteins, but not Sp1 protein, were present in the H_2O_2-inducible probe 3 complex.

Involvement of Egr transcription factors in Cbl-b expression. To investigate Egr-mediated Cbl-b expression, we first measured Egr and Cbl-b mRNA levels in L6 myoblasts after 3D clinorotation. Egr1 and -2 mRNA levels were induced after 90 min of 3D clinorotation or H_2O_2 treatment (Fig. 4, *A* and *B*). Western blotting confirmed 3D clinorotation-induced changes in Egr1 and Egr 2 proteins that correlated well with induction of the transcripts (Fig. 4*C*). We also observed an increase in

Fig. 2. Myo-Lab space and ground experiments. *A*: the thicknesses of L6 myotubes cultured in the Japanese Experimental Module (JEM) of the the International Space Station (ISS) were calculated. *Left*: representative images of myotubes treated as indicated. Scale, 100 μm. *Right*: measurement of diameters as described in MATERIALS AND METHODS. Results are means< SD ($n = 100$). *P< 0.05 vs. 1*G*. *B*: thicknesses of L6 myotubes stimulated with 3-dimensional (3D) clinorotation for 72 h compared with sedentary conditions. *Left*: representative images of myotubes treated as indicated. Scale, 100 μm. *Right*: quantification of diameters as described in MATERIALS AND METHODS. Results are means< SD ($n = 100$). *P< 0.05 vs. sedentary. *C*: levels of myosin heavy chain (MyHC) slow/fast,<-actinin, and<-tubulin in L6 myotubes cultured under the indicated conditions in the JEM of the ISS were assessed by immunoblotting. *D*: metabolomics analysis of L6 myotubes cultured in the JEM under the indicated conditions, measuring the indicated metabolites. Results are means< SD ($n = 3$). *P< 0.05 vs. vehicle. ND, not detected. *E*: to detect oxidative stress, L6 myotubes were pretreated with an oxidative stress-quenching fluorescence reagent, 5 μM CellROX Deep Red, for 30 min before being subjected to 3D clinorotation or H_2O_2 treatment for 24 h. Brightness indicates accumulated oxidative stress in the cells. *Left*: representative imaging of cells treated as indicated: bright-field (*top*) and fluorescence (*bottom*). Scale, 100 μm. *Right*: fluorescence intensity quantified by ImageJ software. *P< 0.05 vs. sedentary. *F*: L6 cells subjected to clinorotation for 24 h or sedentary L6 cells were stained with 5 μM 2′,7′-dichlorodihydrofluorescein diacetate (H2DCFDA; *left*) or 5 μM diaminofluorescein-2 diacetate (DAF-2 DA) with DMSO (*right*) for 1 h and subjected to flow cytometry. L6 cells treated with 50 μM H_2O_2 or 50 μM NONOate served as comparison groups. The percentages represent ratio of cells with fluorescence intensity $>1 \times 10^5$.

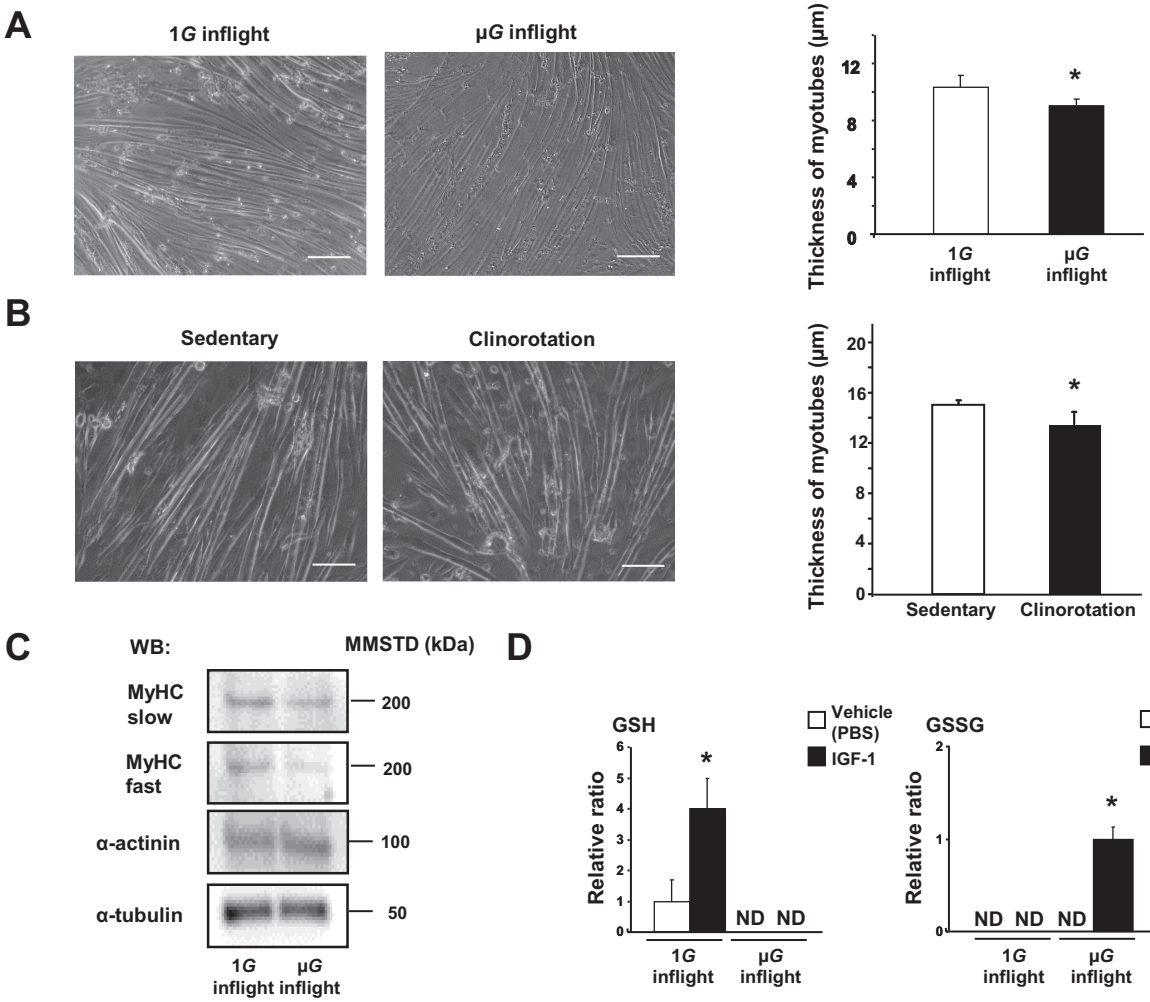

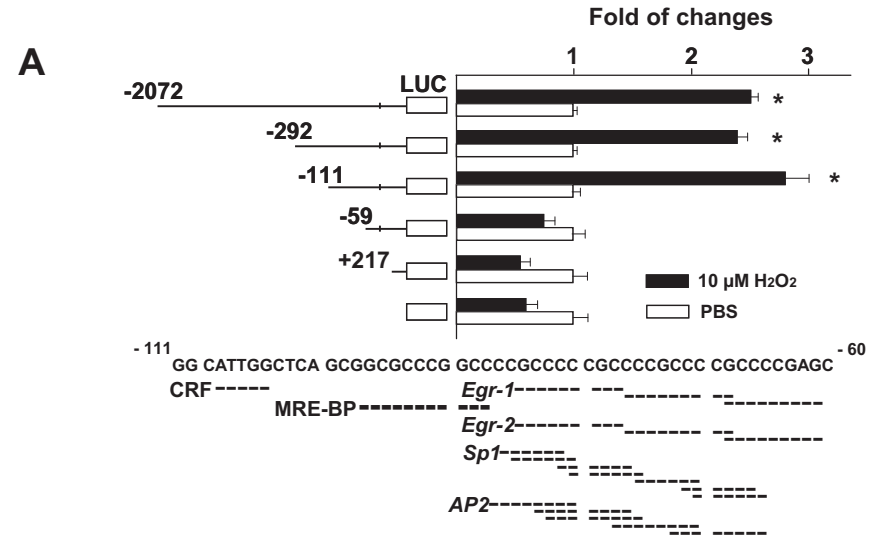

Fig. 3. Egr 1 and Egr 2 are involved in transcriptional upregulation of casitas B-lineage lymphoma-b (Cbl-b) expression in response to oxidative stress. *A*: luciferase assays using luciferase reporter vectors driven by various fragments of the Cbl-b promoter region, with fragments in the 5′-flanking region from −2,072 to +249 bp with respect to the start site. COS7 cells were transfected with the indicated constructs and treated with vehicle (PBS) or 10 μM H_2O_2 for 24 h, followed by evaluation of luciferase activity. Results are means ± SD ($n = 4$). *$P < 0.05$, vehicle vs. H_2O_2. *B*: nuclear extracts (5 μg of protein) from COS7 cells treated with vehicle or 10 μM H_2O_2 were incubated with the indicated isotope-labeled probe or mutant probe (mt) containing a mutation in the first or second Egr1/2-binding site (probe 3-mt1 or -mt2, respectively) and subjected to EMSA. *Right*: addition of Egr1, Egr2, both Egr 2 and -3, or Sp-1 antibody (Ab). Results are representative of three experiments. Black arrows indicate probe 3 or probe3-mt1 bound by and Egr1/2. *Nonspecific bands.

Cbl-b protein that reached the peak value at 1.5 h after clinorotation.

We next determined the importance of Egr transcription factors in clinorotation-induced Cbl-b expression using siRNA constructs targeting Egr1 or -2. Quantitative RT-PCR showed that transfection with siRNAs against Egr1 or -2 mRNA resulted in attenuated expression of the targeted Egr in L6 cells subjected to 3D clinorotation compared with cells transfected with negative control sequences (Fig. 4*C*). Each individual siRNA did not affect Cbl-b mRNA expression during 3D clinorotation. However, simultaneous transfection of both Egr1 and -2 siRNAs significantly decreased clinorotation-induced Cbl-b mRNA expression, suggesting that Egrs compensated for one another in regulating Cbl-b.

Fig. 4. Upregulation of Cbl-b expression induced by 3D clinorotation through Egr1 and Egr2. *A* and *B*: L6 myoblasts were subjected to 3D clinorotation (*A*) or 10 μM H_2O_2 treatment (*B*) for the indicated periods. Levels of Egr1 and Egr2 transcripts were assessed by real-time RT-PCR. The ratios of target transcript levels to those of GAPDH mRNA were calculated. Results are means< SD ($n = 4$). *P< 0.05 compared with untreated cells. *C*: L6 myoblasts were subjected to 3D clinorotation for the indicated periods, and immunoblotting was performed for Egr1, Egr2, and Cbl-b. The immunoblotting results are shown representative of three independent experiments. Graph shows quantification of protein levels. *P< 0.05 compared with before 3D clinorotation. *D*: L6 myoblasts were transfected with siRNAs targeting Egr1, Egr2, both Egr 1 and 2 siRNA ("all"), or negative control siRNA ("nonspecific") for 3 days before 3D clinorotation. Egr 1, Egr 2, and Cbl-b mRNA levels were assessed by real-time RT-PCR. Results are means< SD ($n = 4$). *P< 0.05 before vs. after 3D clinorotation. #P< 0.05, nonspecific RNA vs. siRNA.

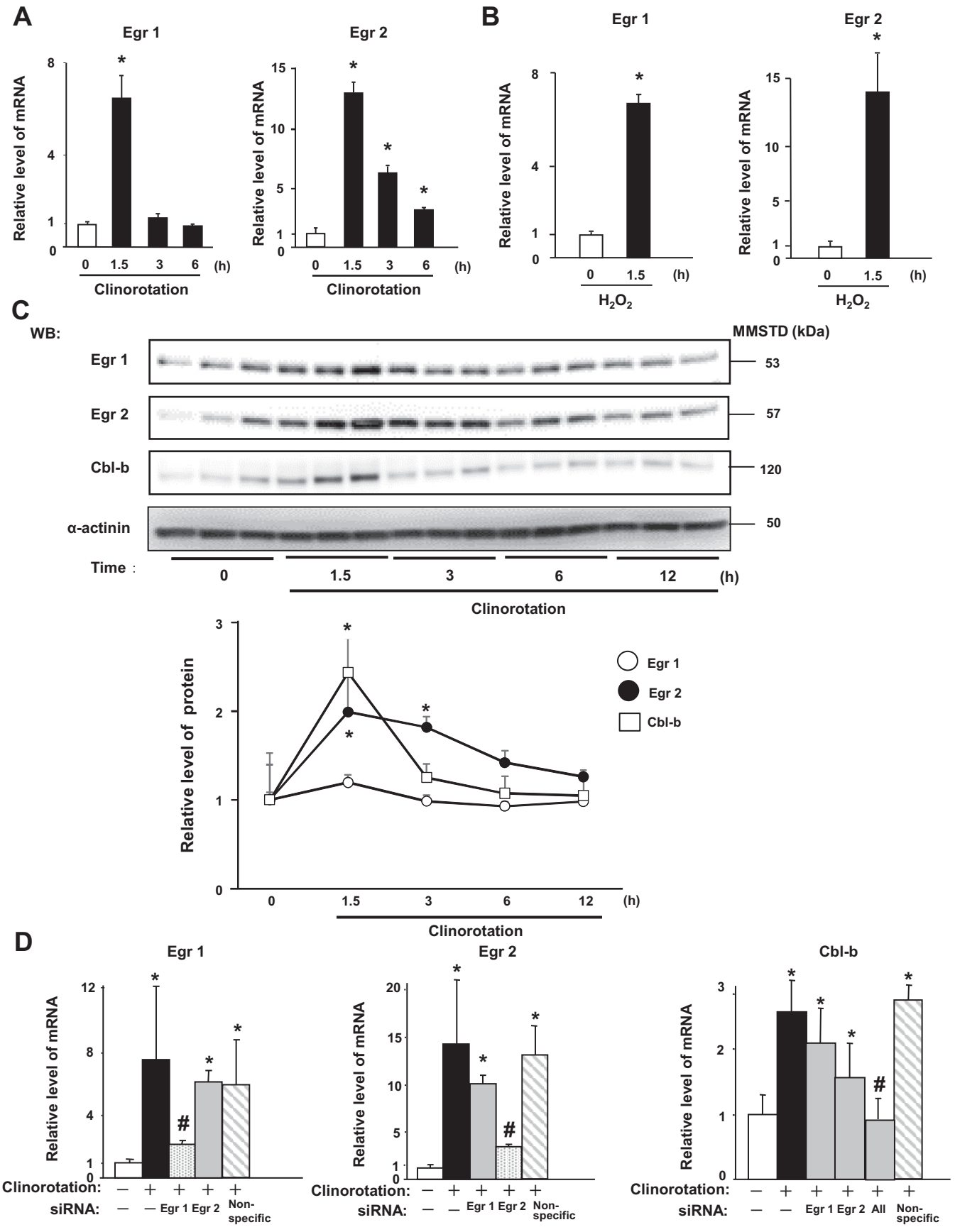

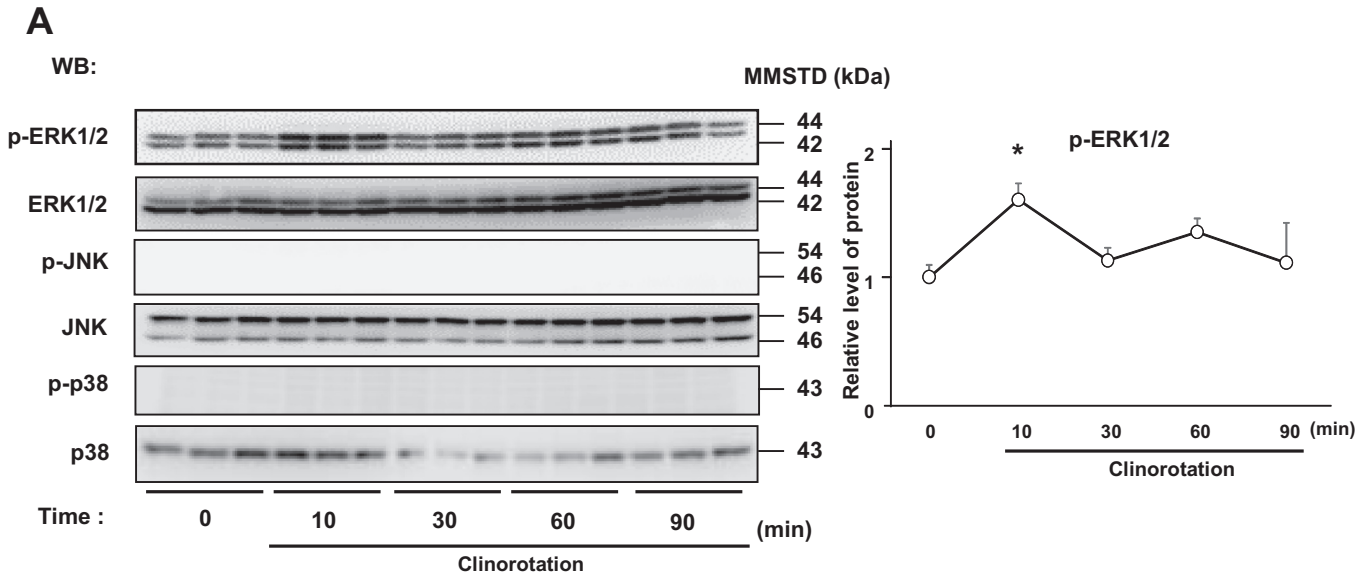

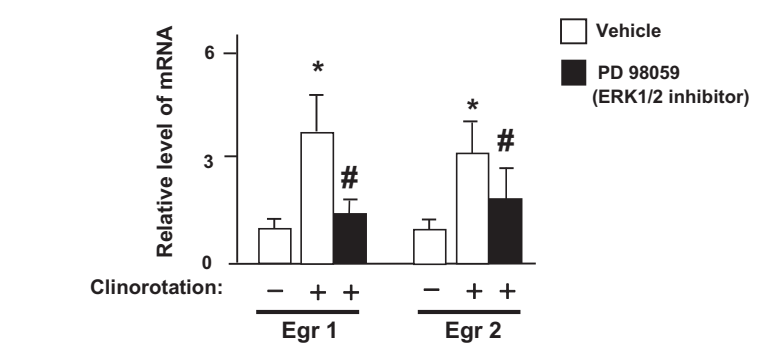

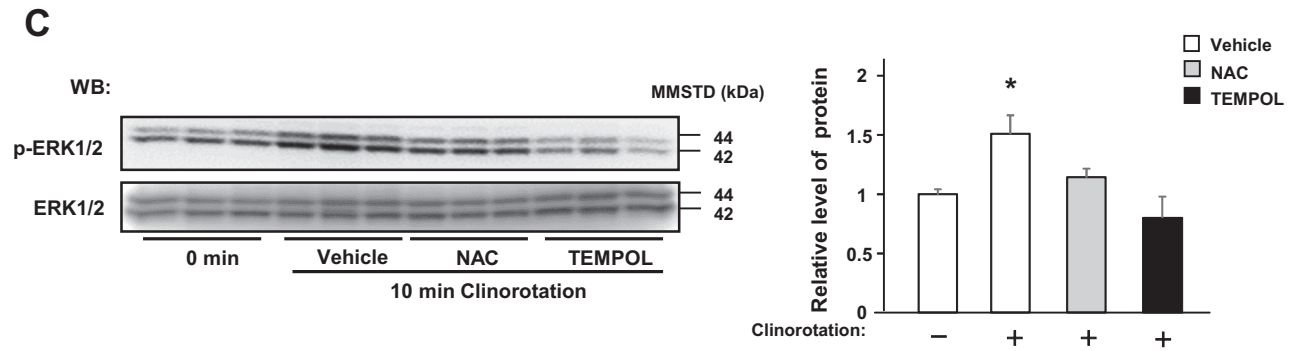

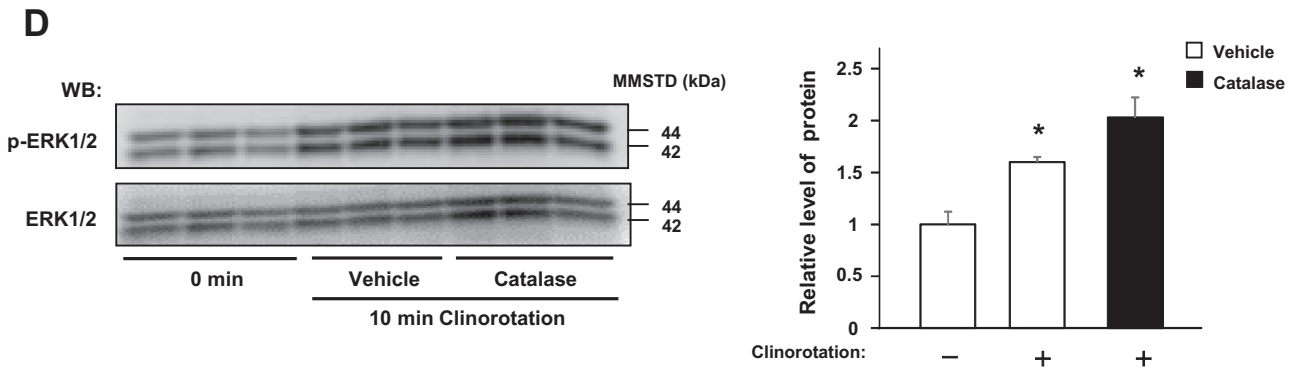

Involvement of oxidative stress in clinorotation-mediated ERK1/2 activation. Because ROS and other stress stimuli activate members of the mitogen-activated family of protein kinases (MAPKs), including ERK1/2, JNK, and p38 (3), we examined the involvement of these kinases in clinorotation-mediated Egr regulation in L6 myotubes. Clinorotation did not affect the amounts of ERK1/2 and JNK in L6 myotubes, whereas the level of p38 significantly decreased at 30 and 60 min after clinorotation (Fig. 5*A*). Interestingly, clinorotation only stimulated phosphorylation of ERK1/2 among the MAPK pathway factors examined; no phosphorylation of JNK or p38 was detected. Furthermore, inhibition of ERK1/2 signaling by the PD-98059 ERK1/2 inhibitor significantly attenuated unloading-induced Egr1 and -2 expression, suggesting that among the MAPK signaling pathways, the ERK1/2 pathway is the most important for the induction of Egr expression possibly by oxidative stress.

To elucidate the involvement of oxidative stress in clinorotation-mediated ERK1/2 activation, we next examined the effects of various antioxidative reagents, including NAC, TEMPOL, and catalase, on clinorotation-mediated phosphorylation of ERK1/2 in L6 myotubes. NAC and TEMPOL significantly suppressed clinorotation-mediated activation of ERK1/2 (Fig. 5*C*), but catalase had no effect (Fig. 5*D*). The suppressive effect of TEMPOL on clinorotation-mediated ERK1/2 activation was stronger than that of NAC. Because TEMPOL mimics superoxide dismutase (30), these results suggest that mitochondria, a most common superoxide supplier, may play an important role in unloading-mediated ROS production.

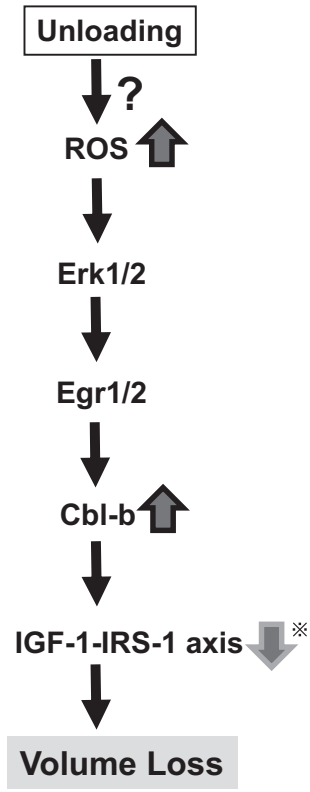

Fig. 6. Mechanistic model of unloading-induced signal induction in skeletal muscle cells. We found that unloading produces reactive oxygen species (ROS) in skeletal muscle cells. ROS increase the transcriptional activity of Egr1 and/or Egr2 to stimulate Cbl-b expression, possibly through the ERK pathway. *Cbl-b consequently induces muscle atrophy through the impairment of IGF-I signaling by IRS-1 ubiquitination and degradation, as reported previously (19).

DISCUSSION

Our study was designed to elucidate the mechanism of the transduction of unloading mechanical stress into catabolic signals, such as the expression of the muscle atrophy-associated ubiquitin ligase Cbl-b (19), in skeletal muscle cells, since skeletal muscle is vulnerable to atrophy under mechanical unloading stress. Recent studies have demonstrated that increased ROS production was important in muscle atrophy associated with disuse (25, 26). In the present study, we elucidated the pathological linkage between simulated and actual microgravity-induced ROS production and expression of the muscle atrophy-associated ubiquitin ligase Cbl-b in skeletal muscle cells.

Our study suggested that ERK1/2 in the MAPK pathway was associated with the oxidative stress that accumulates during unloading. This finding was consistent with other reports showing that oxidative stress was associated with conditions such as muscle atrophy and injury through ERK1/2 activation (6). Furthermore, we found that ERK1/2 activation led to upregulation of Cbl-b expression via the transcription factors Egr1 and -2 (Fig. 5). These findings suggest that increased levels of ROS link mechanical stress to downstream signaling pathways. Consistent with the findings of another laboratory using Egr-knockout mice (27), our Egr knockdown results confirmed that Egr transcription factors play a major role in 3D clinorotation-mediated Cbl-b induction. Egr transcription factors are involved in the response to mechanical stress (6, 10, 22). We found that Egr expression is induced by 3D clinorotation within 90 min of stimulation, indicating that the Egr genes are in close temporal proximity to the mechanical stress "receptor". In addition, we previously demonstrated that elevated Cbl-b interacted with and degraded the IGF-I signaling intermediate IRS-1 (19). Together, our results demonstrated that ROS function as earl upstream mechanotransducers of unloading stress in skeletal muscle. That is, at the

Fig. 5. MAPK signaling pathway and Egr expression in L6 myoblasts subjected to 3D clinorotation. *A*: effects of 3D clinorotation on the MAPK pathway. L6 myoblasts were subjected to 3D clinorotation for the indicated time period. *Left*: extracted proteins (10 μg/lane) were subjected to immunoblotting. Similar results were obtained from three separate experiments. *Right*: quantification of phosphorylated ERK1/2 levels. *$P <$ 0.05 compared with untreated cells. *B*: effects of ERK1/2 inhibitor on Egr expression in L6 myoblasts. L6 myoblasts were pretreated with vehicle (DMSO) or 10 μM PD-98059 (ERK1/2 inhibitor) for 3 h, followed by 3D clinorotation. Egr and GAPDH mRNA levels were assessed by real-time RT-PCR. The ratios of target transcripts to GAPDH mRNA were calculated. Results are means< SD ($n = 4$). *$P <$ 0.05 before vs. after 3D clinorotation; #$P <$ 0.05 compared with vehicle. *C* and *D*: effects of antioxidant on ERK1/2 phosphorylation in L6 myotubes. L6 myotubes were subjected to 3D clinorotation with vehicle (DMSO), 1 mM NAC, 10 mM TEMPOL (*C*), or 200 U/ml catalase (*D*). *Left*: levels of phospho- and total ERK1/2 were assessed by immunoblotting. *Right*: quantification of phosphorylated ERK1/2 levels. *$P <$ 0.05 compared with no 3D clinorotation.

initiation period, ROS is a critical factor inducing the ubiquitination of muscle proteins in unloaded skeletal muscle that, in turn, is associated with unloading-mediated muscle atrophy (Fig. 6). We partially uncovered the molecular mechanism through which mechanical unloading is transduced into biochemical signaling in skeletal muscle.

Recently, several lines of investigation suggested that elevated oxidative stress was not associated with muscle atrophy. Mitochondrial dysfunction elevated oxidative stress but failed to induce muscle atrophy in a young or old mouse model with targeted deficiency of the manganese superoxide dismutase (17). Administration of the antioxidant vitamin E to hindlimb animals, which increased antioxidant defense systems, counteracted muscle fiber type switching phenotype but did not have any impact on muscle atrophy (4). Our results are consistent with the evidence that suppression of oxidative stress in skeletal muscle had beneficial effects against unloading-mediated muscle atrophy (11, 23). One possible explanation to resolve the discrepancies between these results and ours is that the types of ROS induced by distinct unloading conditions may be different. Tail suspension induced the atrophy of mouse soleus and gastrocnemius muscles dominantly through neural nitric oxide synthase-mediated NO production (33), whereas superoxide released from mitochondria by denervation induced muscle atrophy (18). Possibly, nitrogen oxide and/or superoxide elevated at an early stage stimulate ubiquitin ligase expression. To clarify this hypothesis, we performed flow cytometry analysis for ROS detection (Fig. 2*F*) and examined the effects of various antioxidative reagents on clinorotation-mediated ERK1/2 activation (Fig. 5, *C* and *D*). Flow cytometry with a NO-specific fluorescence indicator failed to detect NO after clinorotation. NAC and TEMPOL significantly suppressed clinorotation-mediated activation of ERK1/2, but catalase had no effect. Interestingly, the suppressive effect of TEMPOL on clinorotation-mediated ERK1/2 activation was stronger than that of NAC. Because TEMPOL mimics superoxide dismutase (30), our results suggest that microgravity and clinorotation produce mainly superoxide anions, leading to upregulation of Cbl-b expression in skeletal muscle cells (Fig. 6).

We are currently in the process of identifying the target of the increased ROS. Our preliminary data has indicated that increased ROS inhibits several oxidative stress-sensitive enzymes, such as aconitase, resulting in mitochondrial dysfunction (unpublished observations). In fact, Higashitani et al. (8) reported that actual microgravity significantly suppressed the expression of mitochondrial aconitase in *Caenorhabditis elegans*, suggesting impaired mitochondrial dysfunction. Unloading-mediated muscle atrophy is associated with mitochondrial dysfunction and increased ROS production. However, what factor(s) is involved in unloading-mediated ROS production? It is well known that shear stress induces oxidative stress in various cells, such as endothelial cells (2, 5, 15). Therefore, we examined the effect of microgravity and clinorotation on the amount of α-actinin, a cross-linking cytoskeletal stress marker (13), in L6 myotubes (Fig. 2*C*). Microgravity and clinorotation had little impact on the amounts of α-actinin in L6 myotubes. In addition, low shear stress induces mainly nitrogen oxide (2, 5, 15). These findings indicated that real and simulated microgravity conditions in this study did not cause shear stress. Because the factor(s) or apparatus producing oxidative stress may be the actual mechanosensors linking unloading stress to skeletal muscle atrophy, the next important step is to identify these factors.

ACKNOWLEDGMENTS

We thank K. Fukui, H. Suzuki, and C. Yamazaki at the Japan Space Forum, T. Hashizume at Advanced Engineering Services, and I. Osada at Japan Manned Space Systems for assistance with the Myo-Lab space experiment.

GRANTS

This study was supported primarily by the International Space Experiment Announcement for Space Utilization promoted by the Japan Aerospace Exploration Agency and the Japan Space Forum. In addition, it was partially supported by grants-in-aid for Scientific Research from the Ministry of Education, Culture, Sports, Science, and Technology of Japan (15H04960 and 16H01645) (to T. Nikawa) and by the Japanese Council for Science, Technology, and Innovation Program (14533567) "Technologies for Creating Next-Generation Agriculture, Forestry and Fisheries" (funding agency: Bio-Oriented Technology Research Advancement Institution) (to T. Nikawa).

DISCLOSURES

No conflicts of interest, financial or otherwise, are declared by the authors.

AUTHOR CONTRIBUTIONS

T.U., Y.S., K.K., Y.Y., C.T., Y.K., A.K., T.S., and T.N. performed experiments; T.U., Y.S., Y.Y., Y.K., A.K., K.H., R.N., N.I., T.K., M.O., S.T., E.T., K.T., M.S., and T.N. analyzed data; T.U. and T.N. prepared figures; T.U., E.M.M., and T.N. drafted manuscript; K.K., Y.Y., C.T., Y.K., A.K., K.H., A.O., R.N., A. Higashitani, A. Higashibata, N.I., T.S., T.K., Y.O., I.C., M.O., E.M.M., S.T.-K., S.T., E.T., K.T., M.S., and T.N. interpreted results of experiments; T.N. conceived and designed research; T.N. approved final version of manuscript.

REFERENCES

1. **Bodine SC, Stitt TN, Gonzalez M, Kline WO, Stover GL, Bauerlein R, Zlotchenko E, Scrimgeour A, Lawrence JC, Glass DJ, Yancopoulos GD.** Akt/mTOR pathway is a crucial regulator of skeletal muscle hypertrophy and can prevent muscle atrophy *in vivo*. *Nat Cell Biol* 3: 1014–1019, 2001. doi:10.1038/ncb1101-1014.
2. **Cheng C, van Haperen R, de Waard M, van Damme LC, Tempel D, Hanemaaijer L, van Cappellen GW, Bos J, Slager CJ, Duncker DJ, van der Steen AF, de Crom R, Krams R.** Shear stress affects the intracellular distribution of eNOS: direct demonstration by a novel in vivo technique. *Blood* 106: 3691–3698, 2005. doi:10.1182/blood-2005-06-2326.
3. **Cowan KJ, Storey KB.** Mitogen-activated protein kinases: new signaling pathways functioning in cellular responses to environmental stress. *J Exp Biol* 206: 1107–1115, 2003. doi:10.1242/jeb.00220.
4. **Desaphy JF, Pierno S, Liantonio A, Giannuzzi V, Digennaro C, Dinardo MM, Camerino GM, Ricciuti P, Brocca L, Pellegrino MA, Bottinelli R, Camerino DC.** Antioxidant treatment of hindlimb-unloaded mouse counteracts fiber type transition but not atrophy of disused muscles. *Pharmacol Res* 61: 553–563, 2010. doi:10.1016/j.phrs.2010.01.012.
5. **Dimmeler S, Fleming I, Fisslthaler B, Hermann C, Busse R, Zeiher AM.** Activation of nitric oxide synthase in endothelial cells by Akt-dependent phosphorylation. *Nature* 399: 601–605, 1999. doi:10.1038/21224.
6. **Hasan RN, Schafer AI.** Hemin upregulates Egr-1 expression in vascular smooth muscle cells via reactive oxygen species ERK-1/2-Elk-1 and NF-kappaB. *Circ Res* 102: 42–50, 2008. doi:10.1161/CIRCRESAHA.107.155143.
8. **Higashibata A, Hashizume T, Nemoto K, Higashitani N, Etheridge T, Mori C, Harada S, Sugimoto T, Szewczyk NJ, Baba SA, Mogami Y, Fukui K, Higashitani A.** Microgravity elicits reproducible alterations in cytoskeletal and metabolic gene and protein expression in space-flown *Caenorhabditis elegans*. *NPJ Microgravity* 2: 15022, 2016. doi:10.1038/npjmgrav.2015.22.
9. **Hirasaka K, Nikawa T, Yuge L, Ishihara I, Higashibata A, Ishioka N, Okubo A, Miyashita T, Suzue N, Ogawa T, Oarada M, Kishi K.** Clinorotation prevents differentiation of rat myoblastic L6 cells in association with reduced NF-κ B signaling. *Biochim Biophys Acta* 1743: 130–140, 2005. doi:10.1016/j.bbamcr.2004.09.013.

10. **Huang RP, Adamson ED.** A biological role for Egr-1 in cell survival following ultra-violet irradiation. *Oncogene* 10: 467–475, 1995.
11. **Ikemoto M, Nikawa T, Kano M, Hirasaka K, Kitano T, Watanabe C, Tanaka R, Yamamoto T, Kamada M, Kishi K.** Cysteine supplementation prevents unweighting-induced ubiquitination in association with redox regulation in rat skeletal muscle. *Biol Chem* 383: 715–721, 2002. doi:10.1515/BC.2002.074.
12. **Ikemoto M, Nikawa T, Takeda S, Watanabe C, Kitano T, Baldwin KM, Izumi R, Nonaka I, Towatari T, Teshima S, Rokutan K, Kishi K.** Space shuttle flight (STS-90) enhances degradation of rat myosin heavy chain in association with activation of ubiquitin-proteasome pathway. *FASEB J* 15: 1279–1281, 2001. doi:10.1096/fj.00-0629fje.
13. **Jackson WM, Jaasma MJ, Tang RY, Keaveny TM.** Mechanical loading by fluid shear is sufficient to alter the cytoskeletal composition of osteoblastic cells. *Am J Physiol Cell Physiol* 295: C1007–C1015, 2008. doi:10.1152/ajpcell.00509.2007.
15. **Lee J, Packard RR, Hsiai TK.** Blood flow modulation of vascular dynamics. *Curr Opin Lipidol* 26: 376–383, 2015. doi:10.1097/MOL.0000000000000218.
16. **Lowry OH, Rosebrough NJ, Farr AL, Randall RJ.** Protein measurement with the Folin phenol reagent. *J Biol Chem* 193: 265–275, 1951.
17. **Lustgarten MS, Jang YC, Liu Y, Qi W, Qin Y, Dahia PL, Shi Y, Bhattacharya A, Muller FL, Shimizu T, Shirasawa T, Richardson A, Van Remmen H.** MnSOD deficiency results in elevated oxidative stress and decreased mitochondrial function but does not lead to muscle atrophy during aging. *Aging Cell* 10: 493–505, 2011. doi:10.1111/j.1474-9726.2011.00695.x.
18. **Muller FL, Song W, Jang YC, Liu Y, Sabia M, Richardson A, Van Remmen H.** Denervation-induced skeletal muscle atrophy is associated with increased mitochondrial ROS production. *Am J Physiol Regul Integr Comp Physiol* 293: R1159–R1168, 2007. doi:10.1152/ajpregu.00767.2006.
19. **Nakao R, Hirasaka K, Goto J, Ishidoh K, Yamada C, Ohno A, Okumura Y, Nonaka I, Yasutomo K, Baldwin KM, Kominami E, Higashibata A, Nagano K, Tanaka K, Yasui N, Mills EM, Takeda S, Nikawa T.** Ubiquitin ligase Cbl-b is a negative regulator for insulin-like growth factor 1 signaling during muscle atrophy caused by unloading. *Mol Cell Biol* 29: 4798–4811, 2009. doi:10.1128/MCB.01347-08.
20. **Nikawa T, Ishidoh K, Hirasaka K, Ishihara I, Ikemoto M, Kano M, Kominami E, Nonaka I, Ogawa T, Adams GR, Baldwin KM, Yasui N, Kishi K, Takeda S.** Skeletal muscle gene expression in space-flown rats. *FASEB J* 18: 522–524, 2004. doi:10.1096/fj.03-0419fje.
21. **Ogawa T, Furochi H, Mameoka M, Hirasaka K, Onishi Y, Suzue N, Oarada M, Akamatsu M, Akima H, Fukunaga T, Kishi K, Yasui N, Ishidoh K, Fukuoka H, Nikawa T.** Ubiquitin ligase gene expression in healthy volunteers with 20-day bedrest. *Muscle Nerve* 34: 463–469, 2006. doi:10.1002/mus.20611.
22. **Paron I, D'Elia A, D'Ambrosio C, Scaloni A, D'Aurizio F, Prescott A, Damante G, Tell G.** A proteomic approach to identify early molecular targets of oxidative stress in human epithelial lens cells. *Biochem J* 378: 929–937, 2004. doi:10.1042/bj20031190.
23. **Powers SK, Hudson MB, Nelson WB, Talbert EE, Min K, Szeto HH, Kavazis AN, Smuder AJ.** Mitochondria-targeted antioxidants protect against mechanical ventilation-induced diaphragm weakness. *Crit Care Med* 39: 1749–1759, 2011. doi:10.1097/CCM.0b013e3182190b62.
24. **Powers SK, Wiggs MP, Duarte JA, Zergeroglu AM, Demirel HA.** Mitochondrial signaling contributes to disuse muscle atrophy. *Am J Physiol Endocrinol Metab* 303: E31–E39, 2012. doi:10.1152/ajpendo.00609.2011.
25. **Romanello V, Guadagnin E, Gomes L, Roder I, Sandri C, Petersen Y, Milan G, Masiero E, Del Piccolo P, Foretz M, Scorrano L, Rudolf R, Sandri M.** Mitochondrial fission and remodelling contributes to muscle atrophy. *EMBO J* 29: 1774–1785, 2010. doi:10.1038/emboj.2010.60.
26. **Romanello V, Sandri M.** Mitochondrial biogenesis and fragmentation as regulators of muscle protein degradation. *Curr Hypertens Rep* 12: 433–439, 2010. doi:10.1007/s11906-010-0157-8.
27. **Safford M, Collins S, Lutz MA, Allen A, Huang CT, Kowalski J, Blackford A, Horton MR, Drake C, Schwartz RH, Powell JD.** Egr-2 and Egr-3 are negative regulators of T cell activation. *Nat Immunol* 6: 472–480, 2005. [Erratum in *Nat Immunol* 6: 737, 2005.] 10.1038/ni1193.
28. **Salanova M, Schiffl G, Gutsmann M, Felsenberg D, Furlan S, Volpe P, Clarke A, Blottner D.** Nitrosative stress in human skeletal muscle attenuated by exercise countermeasure after chronic disuse. *Redox Biol* 1: 514–526, 2013. doi:10.1016/j.redox.2013.10.006.
29. **Sandri M, Sandri C, Gilbert A, Skurk C, Calabria E, Picard A, Walsh K, Schiaffino S, Lecker SH, Goldberg AL.** Foxo transcription factors induce the atrophy-related ubiquitin ligase atrogin-1 and cause skeletal muscle atrophy. *Cell* 117: 399–412, 2004. doi:10.1016/S0092-8674(04)00400-3.
30. **Schnackenberg CG, Wilcox CS.** The SOD mimetic tempol restores vasodilation in afferent arterioles of experimental diabetes. *Kidney Int* 59: 1859–1864, 2001. doi:10.1046/j.1523-1755.2001.0590051859.x.
31. **Stitt TN, Drujan D, Clarke BA, Panaro F, Timofeyva Y, Kline WO, Gonzalez M, Yancopoulos GD, Glass DJ.** The IGF-1/PI3K/Akt pathway prevents expression of muscle atrophy-induced ubiquitin ligases by inhibiting FOXO transcription factors. *Mol Cell* 14: 395–403, 2004. doi:10.1016/S1097-2765(04)00211-4.
32. **Sun Z, Guo SS, Fässler R.** Integrin-mediated mechanotransduction. *J Cell Biol* 215: 445–456, 2016. doi:10.1083/jcb.201609037.
33. **Suzuki N, Motohashi N, Uezumi A, Fukada S, Yoshimura T, Itoyama Y, Aoki M, Miyagoe-Suzuki Y, Takeda S.** NO production results in suspension-induced muscle atrophy through dislocation of neuronal NOS. *J Clin Invest* 117: 2468–2476, 2007. doi:10.1172/JCI30654.